

Size dependency of mechanical properties of high purity aluminium foils (doi:10.1016/j.msea.2009.08.016)

M. Lederer, V. Gröger, G. Khatibi, B. Weiss

Leia o artigo e responda às seguintes questões:

1. Quais são os objetivos do artigo e como os autores o justificam?

Por que estudar folhas tão finas é importante?

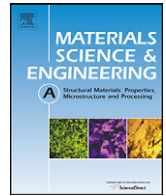
2. Descreva o procedimento experimental empregado.

Como esse procedimento se adequa aos objetivos da pesquisa?

3. Discuta os principais resultados e conclusões apresentados pelos autores.

Avalie como a espessura da folha, o tamanho de grão e a temperatura de ensaio afetam as propriedades mecânicas e como podem afetar a aplicação dessas folhas.

4. Associe os diversos conceitos, resultados e conclusões com o que tem sido apresentado nas aulas.



Size dependency of mechanical properties of high purity aluminium foils

M. Lederer*, V. Gröger, G. Khatibi, B. Weiss

Faculty of Physics at the University of Vienna, Boltzmannngasse 5, A-1090 Wien, Austria

ARTICLE INFO

Article history:

Received 3 February 2009

Received in revised form 9 August 2009

Accepted 10 August 2009

Keywords:

Size effect

Grain size

Surface effect

Tensile test

ABSTRACT

In order to study the size effect, tensile tests with high purity aluminium foils of different thicknesses from 5 μm to 540 μm were performed at room temperature and at 100 °C. A pronounced size effect was observed especially at elevated temperature. There are two major contributions to the size effect: first, the samples get weak if the fraction t/g of thickness t to grain size g is smaller than 1, because the Hall–Petch model can no longer be applied if most of the grain boundaries are at the free surface. Second, the presence of an oxide layer increases the tensile strength of thin foils. Our results are relevant for the prediction of reliability and life time of electronic devices. It may be concluded that the grain size should be refined when the dimensions of electronic parts are reduced.

© 2009 Elsevier B.V. All rights reserved.

1. Introduction

Due to the ongoing miniaturization of electronic parts, the mechanical properties of materials in small dimensions have become increasingly important in recent years. For technical applications like micro-electro-mechanical systems (MEMS) [1] a precise knowledge of yield strength, ultimate tensile strength and fracture strain is required. It is well known that these properties cannot be deduced from experimental data of bulk material [2,3]. Therefore, the materials have to be tested in their actual dimensions.

Starting from the submicron range, the size effect follows the trend smaller is stronger. Filamentary crystals called whiskers [4] were investigated extensively some decades ago. In tensile tests small diameter whiskers nearly achieve the theoretical strength of dislocation free crystals which lies between 0.03 E and 0.17 E. This strength is generally attributed to their perfect structure lacking of mobile dislocations. Similar high strengths were recently reported for single crystal pillar experiments [5–7]. Using a focused ion beam, micron sized aluminium pillars [8] were fabricated showing a strong size effect in compression. The deformation was jerky, and the observed strain bursts were explained by a statistical model.

Furthermore, pronounced thickness effects have been observed in thin aluminium films deposited on a substrate. The flow stress of the films was found to be the sum of strengthening components due to film thickness and presence of grain boundaries [9]. The value for the thickness component of the flow stress was inversely pro-

portional to the film thickness. It was tried to explain the grain size component to the flow stress according to the Hall–Petch relation, but a $1/g$ dependence, where g is the grain size, seemed to be more plausible.

However, the size effect changes its appearance in the thickness range from a few to hundreds of microns. There the dimensional size effect is sometimes overshadowed by the grain size effect [10]. In this range the tensile properties are influenced by the fraction of thickness t to grain size g , which is called t/g . Kotas et al. [11] have measured the low cycle fatigue during loading and unloading of thin copper foils in the tension–tension mode and compared these results to tensile stress–strain curves of identically prepared samples. Since the fracture strain of the thinner samples was lower, the number of cycles to failure during loading and unloading at a given stress was also reduced. Much emphasis was paid to the influence of the fraction t/g on the fatigue properties, where t/g varied from 2 to 6. The samples with smaller t/g clearly showed lower tensile strength and inferior life time.

Janssen et al. [12] have carried out tensile tests with aluminium foils of thicknesses from 100 μm to 340 μm , whereby the grain size varied from 75 μm to 480 μm . Their interpretation of experimental results was also based on the analysis of the fraction t/g of thickness to grain size. If this fraction t/g was ≤ 1 , the samples were weak. Their explanation was that in this case there are soft regions in the core of the grains, where the path of a dislocation along its slip plane does not cross boundaries to neighbouring grains on the way to the sample surface. This interpretation is, however, restricted to the thickness range mentioned by the authors. If the aluminium samples get thinner, the influence of the oxide layer at the surface on the tensile strength increases and should therefore be considered in the model.

* Corresponding author. Tel.: +43 1 4277 51334; fax: +43 1 4277 9513.
E-mail address: martin.lederer@univie.ac.at (M. Lederer).

The role of the aluminium oxide layer was studied by Tabata et al. [13]. They have observed a size effect on the tensile properties of thin aluminium wires in the diameter range from 5 μm to 200 μm with a grain size of about 500 μm . The critical resolved shear stress increased linearly against the inverse square root of the specimen diameter. Based on an electron microscope study, this effect was attributed to the presence of a protecting oxide layer at the surface against which dislocations have to pile up before the sample can deform plastically.

Often a size effect of ductility is observed. If the samples get thinner, the fracture strain is reduced. But this strongly depends on the microstructure: Khatibi et al. [14] have studied the tensile and fatigue properties of Cu micro-wires in the diameter range from 10 μm to 125 μm . After heat treatment a bamboo-like microstructure was achieved where the grain size spanned the entire thickness of the wire. The thinnest samples showed the highest yield strength, the highest fatigue resistance but the lowest fracture strain. The low fracture strain of the 10 μm thin wire (5%) was explained by the fact that 70% of the grains were not deformed at all due to their orientation relative to the tensile axis. However, there are examples where even thin samples reach a surprisingly high fracture strain: Read et al. [15] have reported tensile tests of free standing 1 μm thin Al films with an ultimate tensile strength of 151 MPa and a fracture strain of 22.5%. In their experiment the grain size of 0.3 μm was approximately 1/3 of the thickness.

During tensile testing geometry effects of thin foils are expected. In contrast to thick samples, thin foils may show a buckling behaviour. If different grains deform individually due to their orientations, thin foils do not remain flat. This change of behaviour is sometimes described as transition from plane strain to plane stress deformation [16]. The shape of a possible buckling behaviour depends on length, width, thickness and microstructure of the sample.

A number of theoretical models were proposed in order to explain the size effect. Some of them are based on strain gradient plasticity [17]. The idea behind this theory is that a strain gradient, which may for instance be caused by a nanoindenter in the region around the indent, leads to enhanced hardening due to generation of geometrically necessary dislocations (GNDs). The smaller the indent, the larger is the strain gradient and the density of GNDs. On the other hand, the randomly trapped dislocations occurring in homogeneously strained parts of the specimen are termed statistically stored dislocations (SSDs). Strain gradient theories were successfully applied to nanoindentation experiments [18], microbend tests [19] and torsion of cylindrical bars [20].

In summary, the size effects predicted by strain gradient theories occur at a microscopic length scale. On the other hand, size effects were also observed on a somewhat larger length scale. Whereas the results of strain gradient theories can be summarized as “smaller is stronger”, the size effect at the larger length scale can lead to the opposite behaviour. If the average grain size of a macroscopic sample approaches its thickness, a weakening of the sample is expected. This can be calculated with finite element simulations based on classical continuum mechanics. Hence, there are two kinds of size effects which may lead either to a strengthening or to a weakening of samples. Effects of both kinds were implemented in FEM simulations by Geers et al. [21].

In spite of numerous investigations, some fundamental questions concerning the size dependency of the mechanical properties remained open. First, it is unclear at which thickness range the size effect in the sense “smaller is stronger” begins. Second, only a few investigations deal with the effect of grain size in the range where the fraction t/g is smaller than 1. Third, the contribution of the oxide layer on the surface to the mechanical size effect has so far mostly been discussed on a purely qualitative level. And fourth,

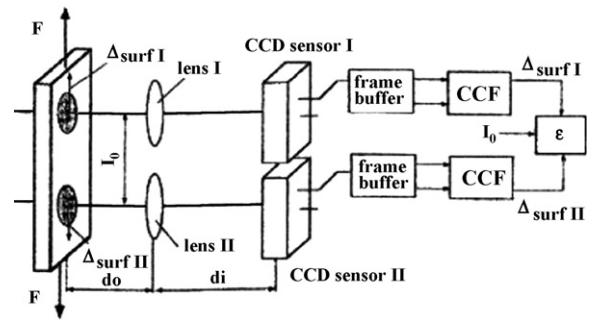


Fig. 1. The laser speckle extensometer schematically [22].

almost nothing is known about a possible temperature dependence of the size effect. Hence, the present study is devoted to the elucidation of these questions. The experiments were carried out with high purity aluminium foils, because this light weight metal is frequently used in the electronic industry. In order to expose the samples to a uniform stress, we have performed tensile tests. Contrary to nanoindentation or bending, the uniaxial tensile test does not directly impose a strain gradient on the sample. This ensures that the observed size effect is an intrinsic property of the sample, but not an effect of the testing method.

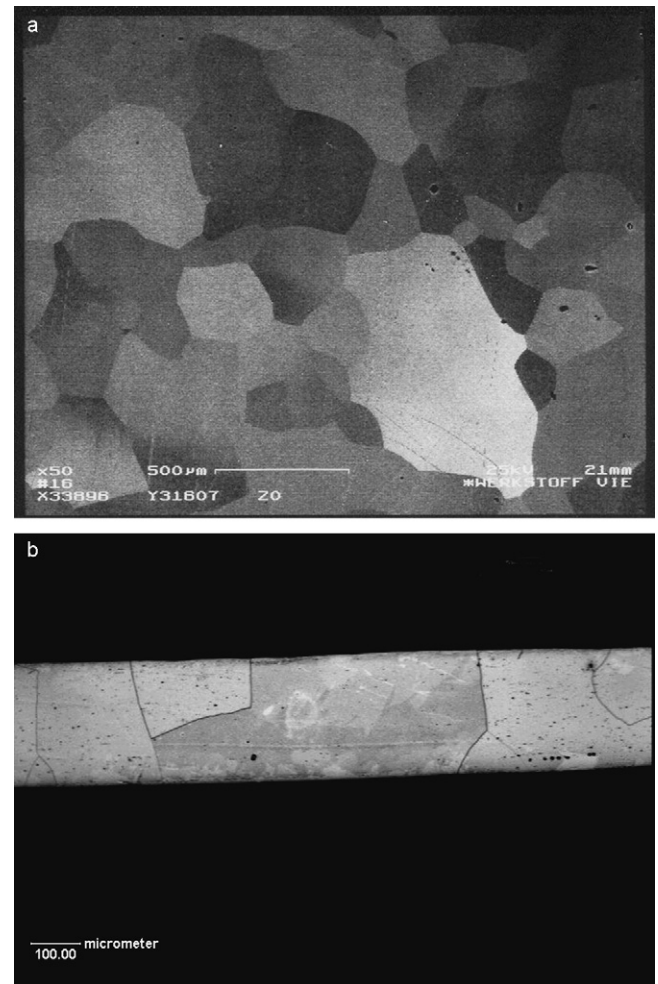


Fig. 2. (a) Microstructure of a 125 μm thick foil after a heat treatment of 2 h at 550 $^{\circ}\text{C}$ (electron back scattering). (b) Cross-section of a 270 μm thick foil after the heat treatment. Most of the grains cross the entire thickness of the sample.

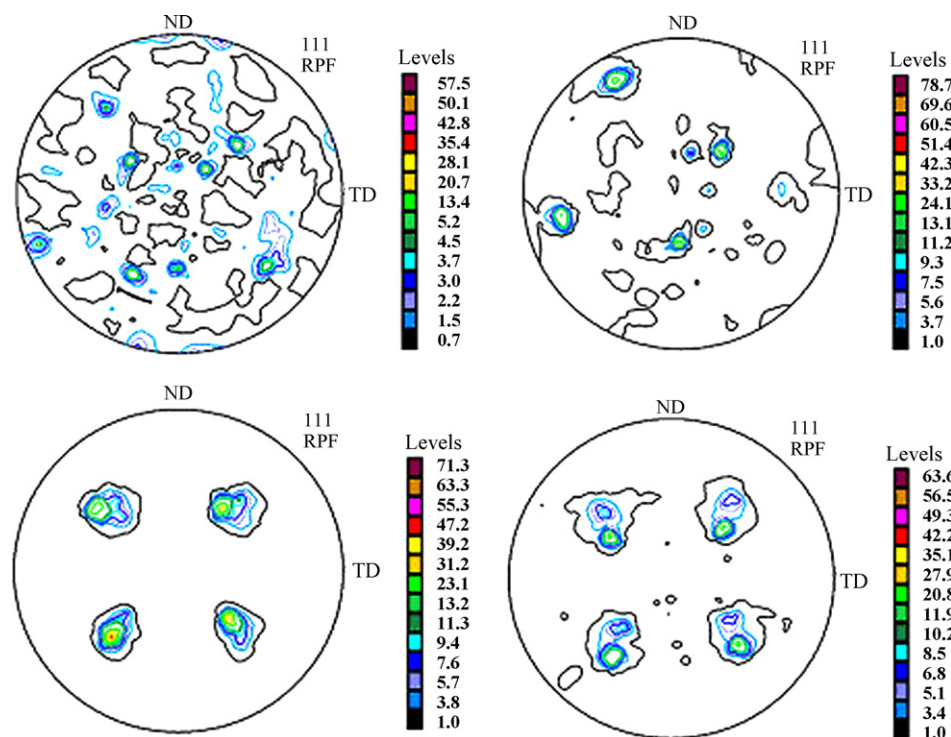


Fig. 3. Textures of a 10 μm (upper left), 20 μm (upper right), 50 μm (lower left) and a 125 μm (lower right) thick foil after the heat treatment. The recalculated pole figures of the 111 reflex are shown.

2. Experimental set-up and sample preparation

2.1. Set-up for tensile tests

A commercial micro tensile machine in combination with 3 different load cells (capacity of 10N, 100N and 500N) suitable for samples of various thicknesses was employed to perform the tensile tests. We have used a laser speckle extensometer [22] as non-contacting optical strain sensor. The arrangement of the laser speckle system is depicted in Fig. 1, schematically: the sample is illuminated by two collimated laser diodes with a distance of 41.74 mm between the two laser spots. The magnified picture of the laser speckle pattern is recorded by two CCD-cameras which are connected to a computer including a frame grabber card for image processing. Thus, the displacement of the pattern is calculated with use of the cross correlation function. The area covered by the cross correlation function is 128×128 pixels for each camera, and the momentary displacement is updated with a frequency of at least 6 Hz. The strain resolution obtained with the help of an algorithm using sub-pixel resolution is better than 1×10^{-5} .

A hot air furnace with slits for the samples was used for the tests at elevated temperature. The sample holders were located outside the furnace avoiding creep within the sample holders during the tensile test. Nevertheless, the strain of the sample was measured inside the furnace through a window of quartz glass. In order to suppress the influence of vibrations in the surrounding, the complete system is stabilized on an optical table standing on a laminar flow isolator.

2.2. Sample preparation, microstructure and texture

Rolled aluminium foils with thicknesses of 5 μm , 10 μm , 20 μm , 48 μm , 125 μm , 270 μm and 540 μm were cut into stripes of 80 mm length and 10 mm width. The purity of the foils in the bulk was 99.999%, but slightly higher surface impurities are possible. After cutting the foils, they were recrystallized for 2 h at 550 $^{\circ}\text{C}$ either in

air or in vacuum. The average grain size after the heat treatment was determined by the line intersection method. An SEM micrograph of a thermal annealed foil can be seen in Fig. 2a. For the coarse grained foils it makes a difference whether the grain size is determined at the rolled surface or at the cross-section of the foil. In the comparison of Table 1 we have used the grain sizes observed at the rolled surface. The cross-section of a 270 μm thick foil is depicted in Fig. 2b. One can see that most of the grains enclose the entire thickness of the sample.

The thickness of the oxide layer after the thermal treatment was determined for a mechanically polished reference sample of the same purity with use of an ellipsometer (type: Plasmos SD 2300 rotating analyser). After heat treatment in air the oxide layer was 27 nm. Since aluminium oxidizes already in the surrounding atmosphere at room temperature, the oxide layer after the heat treatment in vacuum was 5.2 nm.

The texture of the annealed, undeformed samples was recorded with an X-ray goniometer of the type Bruker – AXS – discover 8 with GADDS [23]. The orientation distribution function was calculated with the LaboTex 3.0 software package. Recalculated pole

Table 1

Comparison of grain sizes and textures for Al foils of various thicknesses after thermal treatment. In the thickness range from 48 μm to 540 μm all samples were heat treated in air. The values for the samples from 5 μm to 20 μm thickness refer to heat treatment in vacuum. The corresponding results for heat treatment in air deviate only within statistical error tolerances.

Thickness t	Average grain size g	t/g	Percentage of cubic texture with tolerance angle: $\pm 10^{\circ}$
5 μm	103 μm	0.0485	2.98%
10 μm	797 μm	0.0125	2.5%
20 μm	775 μm	0.026	2.2%
48 μm	128 μm	0.375	58%
125 μm	261 μm	0.479	29%
270 μm	313 μm	0.863	31%
540 μm	540 μm	1	38%

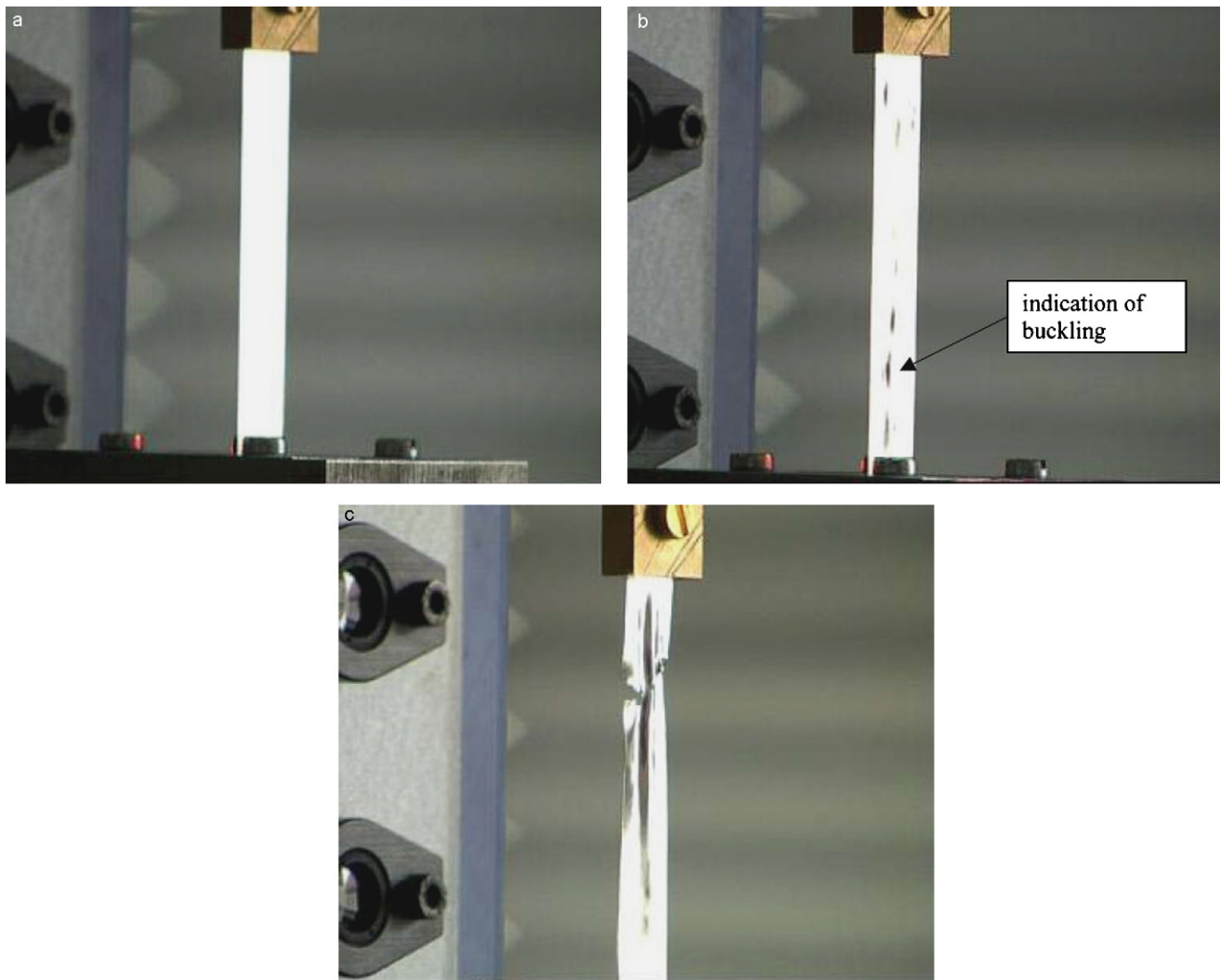


Fig. 4. (a) A 10 μm thin Al foil after heat treatment in vacuum at the beginning of the tensile test. (b) The same foil as in Fig. 4a after plastic deformation during the tensile test. A buckling behaviour occurred already before fracture. (c) A 10 μm thin Al foil heat treated in vacuum at the moment of fracture. During crack propagation the amount of buckling increased, because the local stress in the vicinity of the crack is not uniaxial.

figures of selected samples are depicted in Fig. 3. The percentage of cubic texture using a tolerance angle of $\pm 10^\circ$ for the Euler angles is summarized in Table 1. The foils with thicknesses from 5 μm to 20 μm were randomly textured, whereas the foils with thicknesses from 48 μm to 540 μm showed a pronounced cubic texture. A Goss texture was never observed.

3. Experimental results

For all sample types at least 3 tensile tests were carried out. The tensile direction was always parallel to the rolling direction of the foils. In the thickness range from 48 μm to 540 μm an excellent reproducibility of the experiments was achieved. The thinner foils from 5 μm to 20 μm , however, showed small scattering of the results. This seems to be due to the individual buckling behaviour of these foils which occurred already before rupture (see Fig. 4a–c). All stress–strain curves were analysed with respect to yield strength, strain hardening, ultimate tensile strength and fracture strain.

True stress–strain curves of foils with thicknesses from 48 μm to 540 μm measured at room temperature and at 100 $^\circ\text{C}$ are depicted in Fig. 5a. At room temperature no size effect was observed. The stress–strain curves almost cover each other. However, at 100 $^\circ\text{C}$ a pronounced size effect was found: the thinner foils had lower

ultimate tensile strength. The hardening coefficient $\theta = d\sigma/d\varepsilon$ calculated from true stress–strain curves can be seen in Fig. 5b. For strains above 2% the thicker foils showed more work hardening and finally they reached a higher fracture strain. This effect may be attributed to the microstructure of the foils to some extent. The fraction t/g of thickness to grain size was lower for the thinner foils. A small fraction t/g means that a large part of the grain boundaries is at the free surface of the sample, and this leads to a weakening effect. But on the other hand, the foils tested at room temperature had the same microstructure. So there must be another contribution to the size effect. Therefore, a comparison of the slip band activity at an engineering strain of 10% was carried out for the foils with thicknesses from 125 μm to 540 μm . (see Fig. 6a–e) At room temperature most of the grains showed slip bands along one (37%) or along 2 different directions (40%). Grains with slip bands along 3 directions were rarely seen (7%). Quite often an irregular slip band formation occurred which was due to multiple cross slip (14%). At 100 $^\circ\text{C}$ the percentage of multiple cross slip increased to 45%. The enhanced probability of cross slip seems to be the most significant change of deformation mechanisms caused by elevated temperature.

For the foils from 5 μm to 20 μm thickness there was a strong influence of the oxide layer on the behaviour of the samples. The

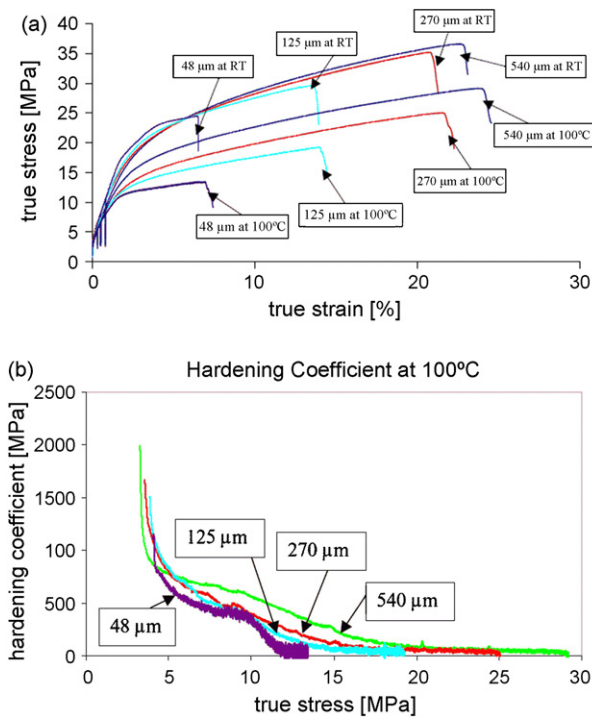


Fig. 5. (a) True stress–strain curves of Al foils from 48 μm to 540 μm thickness. (b) The hardening coefficient $\theta = d\sigma/d\varepsilon$ at 100 $^{\circ}\text{C}$ calculated from true stress strain curves for foils in the thickness range from 48 μm to 540 μm .

results are depicted in Fig. 7a–c. It is interesting that the thickness of the oxide layer had more influence on strain hardening than on the yield strength. In consequence, the ultimate tensile strength of the foils in this thickness range was higher after heat treatment in air.

A comparison of the yield stress measured at a plastic strain of 0.2% is given in Fig. 8. The onset of a size effect in the sense smaller is stronger starts in the thickness range between 20 μm and 50 μm . In general, the yield strength of the foils increases after heat treatment in air compared to foils heat treated in vacuum. But the 5 μm thin foils are an exception to this rule. Due to the different coefficients of thermal expansion of aluminium and the oxide a buckling of the 5 μm thin foils was observed after cooling down from heat treatment in air. Presumably, this has led to generation of misfit dislocations affecting the mechanical behaviour of aluminium. However, this effect was not observed for the foils of 10 μm and 20 μm thickness.

In Fig. 9 a comparison of the ultimate tensile strengths is given. The graph for the UTS of foils heat treated in air shows a minimum for the foils of medium thickness and a maximum for the 5 μm thin foils. The size effect observed is certainly a combined effect of grain size, surface layer and dimensional size effect.

Further, a size effect of fracture strain has been found. The ductility of the thinner foils was drastically reduced (see Fig. 10). In order to investigate the reasons for this behaviour, fracture surfaces were observed with use of an SEM. Typical fracture surfaces of three selected foils are shown in micrographs. In Fig. 11b one can see that fracture occurred in a highly deformed part of an initially 20 μm thick foil, where buckling occurred before rupture. Obviously, the local strain in the region of fracture is much larger than the average strain. These inhomogeneities of strain seem to be responsible for the low ductility of micro-samples.

In Fig. 11c the role of the oxide layer during the process of rupture can be seen. Shreds of the oxide are still present on the sample. But due to the fact that the oxide is only 27 nm thick, the shreds

Table 2

Experimental values of the elastic modulus at room temperature measured during the tensile test by unloading and reloading of the sample. A strong modulus defect was found. In comparison, the ideal Young's modulus along the rolling direction of cubic textured aluminium is approximately 68 GPa.

Foil thickness	Young's modulus at 0.3% plastic strain	Young's modulus at 0.5% plastic strain	Young's modulus at 0.8% plastic strain
540 μm	55.6 \pm 4 GPa	58.2 \pm 4 GPa	54.8 \pm 4.5 GPa
270 μm	54.0 \pm 3 GPa	56.1 \pm 3 GPa	53.2 \pm 3.5 GPa
125 μm	56.5 \pm 4 GPa	60.7 \pm 4 GPa	60.7 \pm 4 GPa
48 μm	58.3 \pm 6 GPa	55.5 \pm 6 GPa	51.0 \pm 7 GPa

cannot consist of oxide only. It seems that pieces of aluminium are attached to the oxide.

The elastic modulus was measured by unloading and reloading during the tensile tests at an engineering strain of 0.3%, 0.5% and 0.8%, respectively. Experimental difficulties have occurred with the foils of 20 μm thickness or thinner because of the buckling behaviour of the foils. If the load is changed abruptly by unloading, the optical sensor cannot reinitialize the reference picture of the speckle pattern fast enough. This leads to a scattering of the results. However, this problem did not occur with the samples of 48 μm thickness or thicker. The results summarized in Table 2 indicate a strong modulus defect.

4. Discussion

According to Arzt [2] size effects of materials can be understood from the point of view of the interaction of a characteristic length with a size parameter. In the present study, the average grain size g is the characteristic length, and the thickness t of the foils is the corresponding dimensional size parameter. If the thickness t approaches the same order of magnitude as the average grain size g , or if the thickness is even smaller than the grain size, a size effect can be expected.

At first we deal with the size effect of the yield strength: for bulk material, the grain size dependence of the yield strength is usually described by the Hall–Petch [24,25] relation. But if the fraction t/g of thickness to grain size is ≤ 1 , this relation has to be modified. In fact, Petch has assumed that the dislocations pile up against the grain boundaries before plastic deformation can take place. But if most of the grains are located at the free surface, the dislocations might escape there. Therefore, samples with $t/g \leq 1$ get weaker.

On the other hand, the surface of the aluminium foils is covered by a strong oxide layer. Tabata et al. [13] have observed dislocation pileups in front of the oxide layer in aluminium wires. Unless the resistance of the oxide layer seems to be smaller than that of a grain boundary, the stress required to push the dislocations through that layer can be high, because the length of the pileup is limited by the thickness of the specimen. The influence of the oxide layer increases with decreasing sample thickness.

In the following a quantitative interpretation of the grain size effect is proposed. At first, it should to be realized that the grain size is ill defined, if one just considers the values measured at the rolled surface. In fact, the grains have pancake geometry, and the grain size along the thickness direction is smaller than the corresponding g -values of Table 1. Since we want to take over a pileup model, we need some size parameter p indicating the possible pileup length within a grain. Let us consider a pileup of edge dislocations in a slip system with high Schmid factor where the angle between slip direction and tensile direction is 45° . Then the possible length of this pileup depends on g , t and the orientation angle α depicted in Fig. 12

a. The angle α is defined in the projection on the plane normal to the tensile direction. With respect to this angle α the length of the pileup is either limited by g or by its intersection with

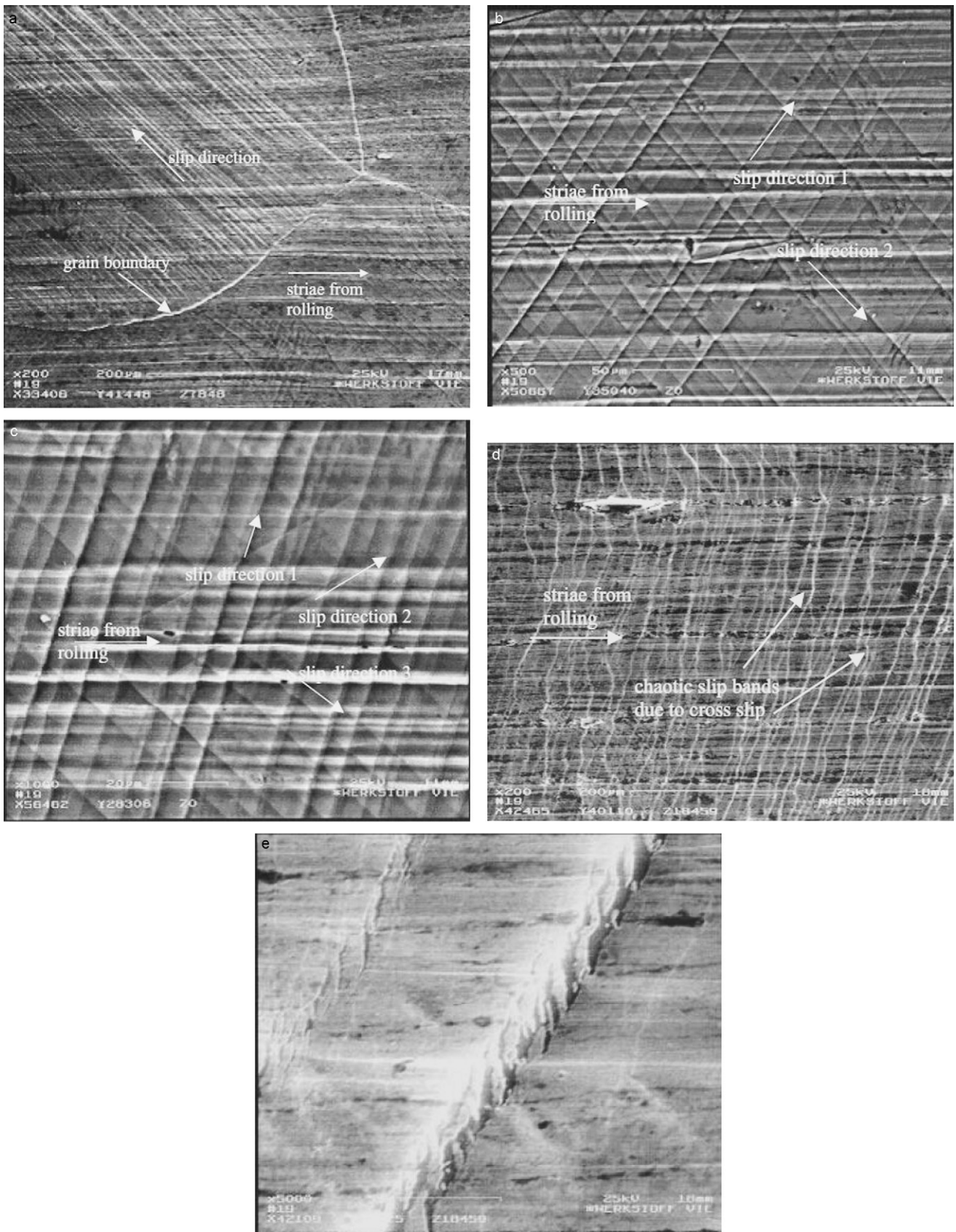


Fig. 6. (a) SEM micrograph of slip band formation in a 540 μm thick foil stretched to an engineering strain of 10% at room temperature. In the large grain (left top) there are slip bands oriented along one direction. The horizontal lines are striae from rolling. (b) Slip bands oriented along 2 different directions in a 270 μm thick foil stretched to an engineering strain of 10% at room temperature. (c) Slip bands oriented along 3 directions in a 125 μm thick foil stretched to an engineering strain of 10% at room temperature. (d) Chaotic slip band formation due to multiple cross slip in a 540 μm thick foil stretched to an engineering strain of 10% at 100 °C. (e) Slip bands in a 540 μm thick foil stretched to an engineering strain of 10% at 100 °C. Under a magnification of 5000× one can see the high deformation along these lines. One can guess that the oxide layer has cracked there, but it has recovered due to oxidation in the surrounding atmosphere.

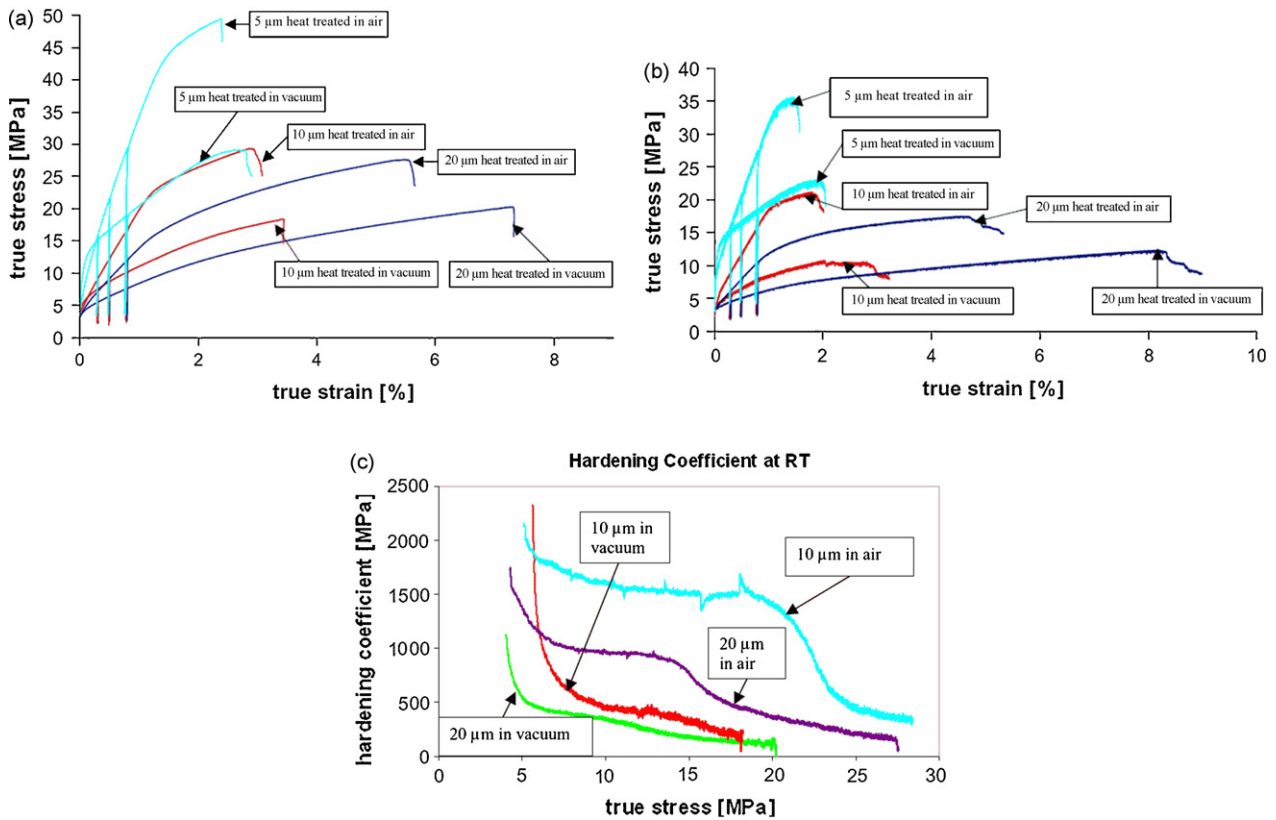


Fig. 7. (a) True stress–strain curves of Al foils with thicknesses of 5 μm, 10 μm and 20 μm at room temperature. (b) True stress–strain curves of Al foils with thicknesses of 5 μm, 10 μm and 20 μm at 100 °C. (c) The hardening coefficients for 10 μm and 20 μm thick foils at room temperature. The foils showed higher strain hardening after heat treatment in air.

the surface. We therefore define the angle $\alpha' = \arcsin(t \cdot \sqrt{2}/g)$ for grain sizes $g \geq t \cdot \sqrt{2}$. Thus, one gets a pileup length of $p=g$ for $0 < \alpha < \alpha'$ and $p = \sqrt{2} \cdot t/\sin(\alpha)$ for $\alpha' < \alpha < \pi/2$. Now we are in the position to evaluate the average value \bar{p} for $0 < \alpha < \pi/2$ from the assumption that the orientation angle α is randomly distributed within this interval. The explicit expression for \bar{p} is given in Appendix A.

On the basis of this pileup length parameter \bar{p} one can interpret the yield strength of the aluminium foils with the modified Hall–Petch relation:

$$\sigma_{yield} = \sigma_0 + \frac{k}{\sqrt{\bar{p}}} \quad (1)$$

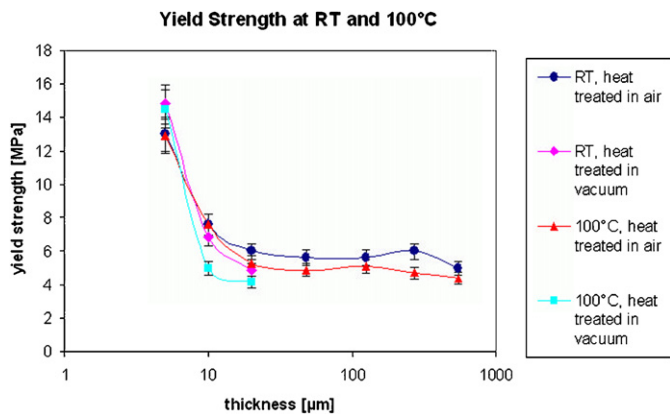


Fig. 8. Comparison of the yield strengths of various Al foils. The yield strength was defined as the flow stress at a plastic strain of 0.2%.

A numerical fit of this model to the experimental data for foils heat treated in air and tested at room temperature is shown in Fig. 13. The experimental results for foils heat treated in vac-

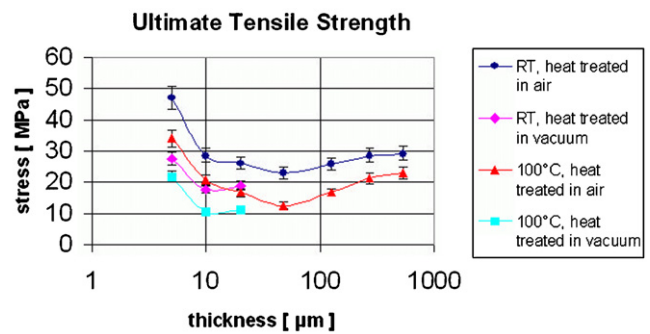


Fig. 9. Diagram of the ultimate tensile strengths versus thickness of the Al foils.

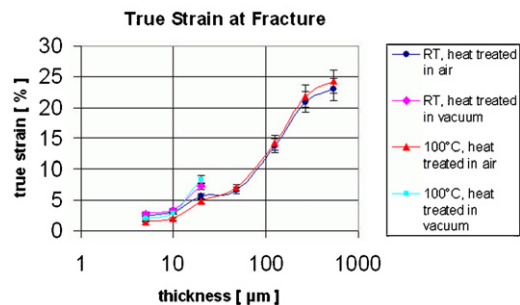


Fig. 10. Comparison of the ductility for foils of various thicknesses.

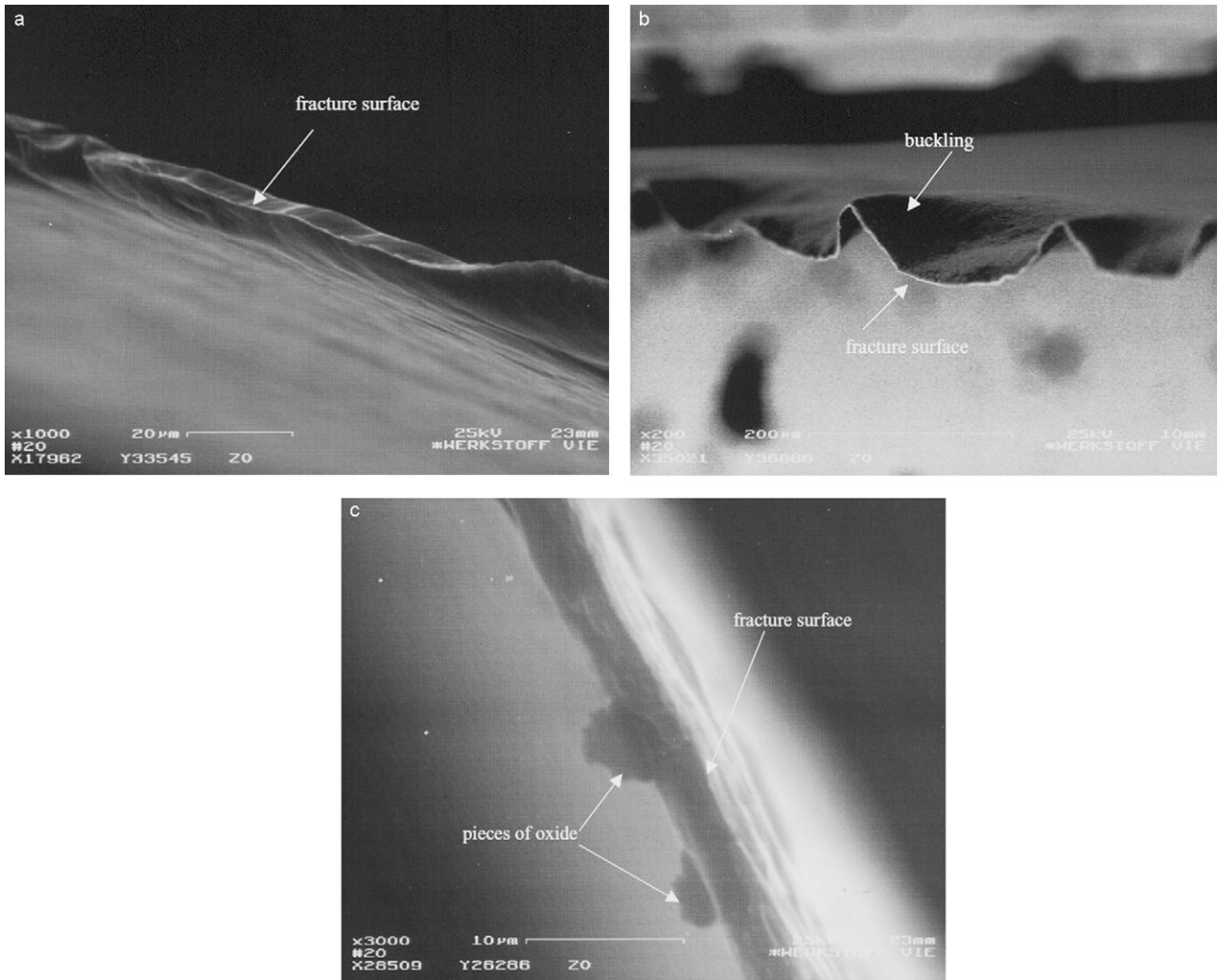


Fig. 11. (a) A 10 μm thick Al foil which was heat treated in vacuum before the tensile test. The fracture surface has the shape of a knife edge. (b) Fracture surface of a 20 μm thick Al foil which was heat treated in vacuum before the tensile test. Rupture occurred in a region where pronounced buckling was observed. (c) A 5 μm thin Al sample which was heat treated in air before the tensile test. Shreds of the oxide layer are still connected to the sample.

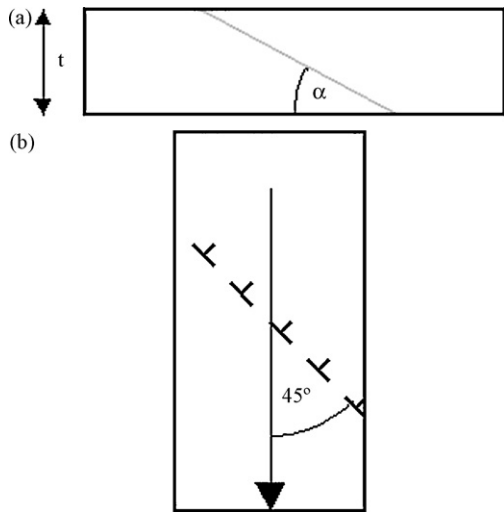


Fig. 12. (a) The orientation angle α is defined in the projection on the plane normal to the tensile direction. The length of a dislocation pileup is either limited by the average grain size g or by the intersection of the pileup with the surface. (b) The angle between pileup direction and tensile direction is assumed as 45° .

uum or tested at 100°C are shown for comparison. The model explains the strong increase of the yield strength for thin aluminium foils although the grain sizes g are rather large. Indeed, the oxide layer at the surface plays the role of a barrier against which

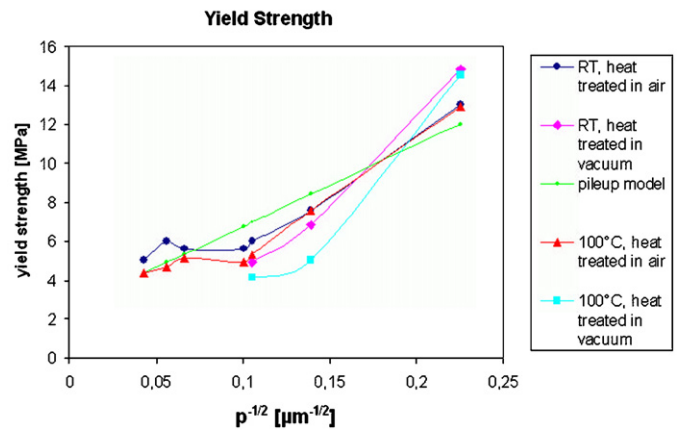


Fig. 13. The combined grain size and thickness effect on the yield strength is compared to the pileup model. The pileup length parameters \bar{p} for the foils of 5 μm, 10 μm, 20 μm, 48 μm, 125 μm, 270 μm and 540 μm thickness are 19.679 μm, 51.541 μm, 90.096 μm, 99.494 μm, 229.542 μm, 313 μm and 540 μm, respectively.

dislocations pile up. Nevertheless, there is a difference of the resistance to the dislocation motion arising either from grain boundaries or from the oxide layer. This is the main reason why the theoretical curve of Fig. 13 shows some deviation compared to the experiments.

Moreover, another contribution to the size effect of the yield strength has to be considered. If one compares the foils of 5 μm and 10 μm thickness heat treated in vacuum, then one recognises a distinct increase of the yield strength for the 5 μm thin foil which cannot be explained by a pileup model. This increase might be due to a lack of well placed dislocation sources. Certainly there is an increased demand for dislocation sources in thin samples, because the motion of single dislocations covers only a short distance there. However, we do not expect dislocation starvation in 5 μm thin foils, because the observed yield strength is far below the theoretical strength of a dislocation free crystal. It seems that there are still plenty of dislocation sources in not so well placed positions. But the activation of these sources requires additional energy due to lower Schmid factors of the slip systems or due to a higher backstress obstructing the sources.

In the following, the size effect in the plastic range of deformation is discussed. We start with the thickness range from 5 μm to 20 μm . As a matter of fact, the influence of the oxide layer on strain hardening is higher than its influence on the yield strength. It is well known that misfit dislocations occur in aluminium at the boundaries to its oxide. During plastic deformation, the misfit dislocations participate in dislocation multiplication. Therefore, thin foils with an oxide layer of 27 nm developed a high dislocation density during the tensile test leading to high values of the ultimate tensile strength.

In the thickness range from 48 μm to 540 μm the samples behaved similar as bulk material at room temperature. The stress strain curves agree with a model of Thompson et al. [26], which is an extension of Ashby's theory [27]. In this composite model two regions are distinguished within the grains, whereby the region at the grain boundaries is dominated by GNDs, whereas the core region in the interior of the grains is dominated by SSDs. At an engineering strain of 6% the experimental stress–strain curves of the present study crossed each other. The foils with the smaller grain size showed the higher yield strength but the lower ultimate tensile strength. In the framework of the model in reference [26] this may be explained by the fact that in samples with small grain size there is a higher initial dislocation density but a lower rate of strain hardening. The high initial dislocation density in small grains is a consequence of the surface to volume ratio of grains, because dislocation sources are located along the grain boundaries. The rate of strain hardening is related to the distance SSDs can move before they are trapped. In large grains there is a higher probability that dislocations are trapped before they reach the boundary. This increases the density of SSDs and leads to higher strain hardening.

However, at 100 °C the foils of this thickness range exhibited a pronounced size effect. It seems that at room temperature the surface layer of the foils acted similar as a grain boundary, whereas at 100 °C it became more permeable to the dislocation motion. This might be due to the enhanced probability of cross slip at 100 °C, which we have seen in the slip band observations. At elevated temperature it is easier for the dislocations to bypass obstacles. Therefore, the surface layer can contribute to the temperature dependence of the size effect. During plastic deformation the oxide layer breaks up along slip bands [28]. Although the oxide recovers quickly in the surrounding atmosphere, some gaps in the surface layer persist for couples of seconds. If a dislocation can move through such a gap by cross slip, the resistance to the dislocation motion is reduced. Furthermore, dislocations can also circumvent surface impurities with the help of this cross slip mechanism. The

overall percentage of dislocations which can bypass obstacles at the sample surface depends on the fraction t/g , because only a part of the dislocations gets to the surface. This explains why softening of the material by the cross slip mechanism induces a size effect.

As already mentioned the foils with thicknesses from 5 μm to 20 μm showed a buckling behaviour. If the buckling occurs already before rupture, the reason for this behaviour can be attributed to the plastic anisotropy of the grains. At the onset of plastic deformation at low strain most of the individual grains try to deform by single glide, because the critical resolved shear stress is reached just for one glide system per grain. However, the deformation due to single glide violates the compatibility condition of neighbouring grains. As a consequence, during the ongoing deformation a buckling of the foil can appear. According to the Euler–Bernoulli theory of beams, the force necessary for elastic bending increases with the third power of the thickness, if length and width are kept constant. Therefore, the buckling of the foils was suppressed for the thicknesses from 48 μm to 540 μm .

All foils in the thickness range from 5 μm to 20 μm showed buckling already before rupture. However, the amount of buckling always increased after crack propagation started. In the vicinity of a crack the local state of stress is no longer uniaxial. This leads to an increased buckling as can be seen in Fig. 4c.

An elastic modulus defect in deformed metals was reported by several authors [29–31]. For tensile tests the most relevant contribution to the modulus defect seems to be the reversible motion of dislocations which bow under mechanical stress. This leads to a reduction of the measured value of the Young's modulus. Indeed, the values for the modulus defect of our experiments are surprisingly high. Values of about half the amount were found for 2S aluminium by Hordon et al. [29]. Due to their interpretation the modulus defect $\Delta E/E$ should approximately be proportional to $N \cdot d^3$, where N is the dislocation density and d is the average distance of a dislocation segment between two pinned points. Hordon et al. have found a maximum of the modulus defect at 0.1% plastic strain. Due to the higher purity of our samples, the average distance d between pinning points should increase. In high purity aluminium, dislocations are pinned between forest dislocations. Since the grains of our foils are not embedded in a three-dimensional matrix, the constraints along the grain boundaries are relaxed. Therefore, the grains of our samples can deform by single slip for a longer period and the onset of multiple slip is shifted to a higher strain compared to bulk material. This should shift the maximum of $N \cdot d^3$ to higher strains. As a result, the modulus defect is increased.

5. Summary and conclusions

The size effect of the tensile properties of aluminium foils in the thickness range from 5 μm to 540 μm is a combined dimensional, grain size and surface layer effect which also depends on temperature. This implies the necessity to record the experimental data for any sample dimension of interest. It is insufficient just to interpolate the data over a wide range of thicknesses. In fact, the lowest value for the UTS was found for the samples of medium thickness.

In the thickness range from 48 μm to 540 μm the dimensional size effect was overshadowed by the grain size effect. A small fraction t/g of thickness to grain size leads to a softening of the samples. This behaviour was influenced by unexpected temperature dependence due to enhanced probability of cross slip at elevated temperature.

In the thickness range from 5 μm to 20 μm there was the onset of a size effect in the sense “smaller is stronger”. This effect was mainly driven by the presence of a strong oxide layer. In

comparison to most other metals the effect of this surface layer is more pronounced in aluminium, since aluminium oxidizes rapidly in the surrounding atmosphere and because aluminium oxide is much stronger than pure aluminium.

Our results are of importance for the prediction of the reliability of electronic devices. Coarse grained foils might be the weakest link terminating the life time of electronic parts. It may be concluded that the grain size of the material should be refined when the dimensions of electronic parts are reduced. However, the strength of thin foils can be enhanced by a protecting oxide layer.

Acknowledgements

We like to acknowledge the help of Dr. E. Schafner who has recorded the textures of the samples by X-ray. This work was supported by the FWF under grant 14732.

Appendix A.

For grain sizes $g < t \cdot \sqrt{2}$ one gets $\bar{p} = g$. Otherwise, the average value \bar{p} is derived by the following calculation: in the interval $0 < \alpha < \alpha'$ the average value for p is given by $\bar{p} = g$. For $\alpha' < \alpha < \pi/2$ the average value of p is calculated from the equation:

$$\bar{p} = \frac{\int_{\alpha'}^{\pi/2} \sqrt{2} \cdot t / \sin(\alpha) d\alpha}{\pi/2 - \alpha'} \quad (\text{A1})$$

There from, one obtains

$$\bar{p} = \frac{\sqrt{2} \cdot t \cdot (\ln(\cos(\arcsin(\sqrt{2} \cdot t/g)/2)) - \ln(\sin(\arcsin(\sqrt{2} \cdot t/g)/2)))}{\pi/2 - \arcsin(\sqrt{2} \cdot t/g)} \quad (\text{A2})$$

and the average value \bar{p} for the whole interval $0 < \alpha < \pi/2$ reads as

$$\bar{p} = \frac{g \cdot \arcsin\left(\frac{\sqrt{2} \cdot t}{g}\right) + \sqrt{2} \cdot t \cdot \left(\ln\left(\cos\left(\frac{\arcsin\left(\frac{\sqrt{2} \cdot t}{g}\right)}{2}\right)\right) - \ln\left(\sin\left(\frac{\arcsin\left(\frac{\sqrt{2} \cdot t}{g}\right)}{2}\right)\right) \right)}{\frac{\pi}{2}}$$

References

- [1] T. Conolly, P.E. McHugh, M. Bruzzi, *Fatigue Fract. Eng. Mater. Struct.* 28 (2005) 1119–1152.
- [2] E. Arzt, *Acta Mater.* 46 (16) (1998) 5611–5626.
- [3] G. Dehm, Ch. Motz, Ch. Scheu, H. Clemens, P.H. Mayrhofer, Ch. Mitterer, *Adv. Eng. Mater.* 8 (11) (2006) 1033–1045.
- [4] S.S. Brenner, *Factors Influencing the Strength of Whiskers*, Chapter 2, *Fiber Composite Materials*, ASM, 1965, pp. 11–36.
- [5] M.D. Uchic, D.M. Dimiduk, J.N. Florando, W.D. Nix, *Science* 305 (2004) 986.
- [6] J.R. Greer, W.C. Oliver, W.D. Nix, *Acta Mater.* 53 (2005) 1821–1830.
- [7] W.D. Nix, J.R. Greer, G. Feng, E.T. Lilleodden, *Thin Solid Films* 515 (2007) 3152–3157.
- [8] K.S. Ng, A.H.W. Ngan, *Acta Mater.* 56 (2008) 1712–1720.
- [9] R. Venkatraman, J.C. Bravman, *J. Mater. Res.* 7 (8) (1992) 2040–2048.
- [10] M. Klein, A. Hadrboletz, B. Weiss, G. Khatibi, *Mater. Sci. Eng. A* 319–321 (2001) 924–928.
- [11] A. Kotas, A. Hadrboletz, G. Khatibi, B. Weiss, *Fatigue 2002 Proceedings*, vol. 2, 2002, pp. 859–866.
- [12] P.J.M. Janssen, Th.H. de Keijser, M.G.D. Geers, *Mater. Sci. Eng. A* 419 (2006) 238–248.
- [13] T. Tabata, H. Fujita, S. Yamamoto, T. Cyoji, *J. Phys. Soc. Jpn.* 40 (3) (1976) 792–797.
- [14] G. Khatibi, A. Betzwar-Kotas, V. Gröger, B. Weiss, *Fatigue Fract. Eng. Mater. Struct.* 28 (2005) 723–733.
- [15] D.T. Read, Y.W. Cheng, R.R. Keller, J.D. McColskey, *Scr. Mater.* 45 (2001) 583–589.
- [16] W.D. Callister, *Fundamentals of Materials Science and Engineering*, second edition, Wiley, 2005.
- [17] N.A. Fleck, J.W. Hutchinson, *J. Mech. Phys. Solids* 41 (12) (1993) 1825–1857.
- [18] W.D. Nix, H. Gao, *J. Mech. Phys. Solids* 46 (1998) 411–425.
- [19] J.S. Stölken, A.G. Evans, *Acta Mater.* 46 (1998) 5109–5115.
- [20] N.A. Fleck, G.M. Muller, M.F. Ashby, J.W. Hutchinson, *Acta Metall. Mater.* 42 (1994) 475–487.
- [21] M.G.D. Geers, W.A.M. Brekelmans, P.J.M. Janssen, *Int. J. Solids Struct.* 43 (2006) 7304–7321.
- [22] M. Anwender, B. Zagar, B. Weiss, H. Weiss, *Exp. Mech.* 40 (1) (2000) 98–105.
- [23] K. Helming, M. Lyubchenko, B. He, U. Preckwinkel, *Powder Diffract.* 18 (2) (2003) 99–102.
- [24] E.O. Hall, *Proc. Phys. Soc.* B64 (1951) 747.
- [25] N.J. Petch, *J. Iron Steel Inst.* 174 (25) (1953).
- [26] A.W. Thompson, M.I. Baskes, W.F. Flanagan, *Acta Metall.* 21 (1973) 1017–1028.
- [27] M.F. Ashby, *Phil. Mag.* 21 (1970) 399–424.
- [28] T. Mukai, *J. Sci. Hiroshima Univ. Ser. A* 22 (2) (1958) 99–113.
- [29] M.J. Hordon, B.S. Lement, B.L. Averbach, *Acta Metall.* 6 (1958) 446–453.
- [30] T.S. Ke, *Phys. Rev.* 71 (1947) 533.
- [31] A.D.N. Smith, *Phil. Mag.* 44 (1953) 453–466.